ELSEVIER

International Journal of Mass Spectrometry 185/186/187 (1999) 507–515

International Journal of Mass Spectrometry

Ion mobility studies of metal-coated fullerenes

James L. Fye, Martin F. Jarrold*

Department of Chemistry, Northwestern University, 2145 Sheridan Road, Evanston, IL 60208, USA

Received 9 June 1998; accepted 5 August 1998

Abstract

Ion mobility measurements have been used to examine the structures and fragmentation processes of $Nb_xC_{60}^+$ complexes with up to five niobium atoms. Our results confirm the observations of Martin and collaborators that loss of C_3 is an important fragmentation process for complexes with $x \geq 3$. However, ion mobility measurements for $Nb_xC_{60}^+$ complexes and their $Nb_xC_{60-3n}^+$ fragments show that they are all fullerenes. It is likely that the $Nb_xC_{60-3n}^+$ fragments with an odd number of carbon atoms are stabilized by a niobium atom occupying the defect site in the fullerene cage, and that this stabilization makes C_3 loss energetically favored over the usual fullerene dissociation process of C_2 loss. Detailed analysis of the ion mobility measurements shows that the niobium atoms in the $Nb_xC_{60}^+$ complexes are clustered together on the fullerene surface. At high injection energies a structural transformation occurs for $Nb_2C_{60}^+$ and one of the niobium atoms apparently moves to an endohedral position. This process does not occur for NbC_{60}^+, but an analogous structural transformation appears to occur for all complexes with $x > 2$. (Int J Mass Spectrom 185/186/187 (1999) 507–515) © 1999 Elsevier Science B.V.

Keywords: Ion mobility; Fullerenes; Metal-coated fullerene; Endohedral fullerene

1. Introduction

Studies of nonendohedral metal-C_{60} complexes provide information about metal-fullerene interactions. Early studies for MC_{60}^+ ions showed that for M = Fe, Co, Ni, Cu, Rh, and La the complexes dissociate by breaking the metal-fullerene bond [1]. AgC_{60}^+ and $Ag_3C_{60}^+$ dissociate in a similar way [2]. A few years ago, Martin and co-workers developed a source where enough metal atoms could be added to completely cover the surface of the fullerene and even make several metal layers. They have reported a number of fascinating studies of these metal-coated fullerenes. For example, $Li_7C_{60}^+$ and $Li_{12}C_{60}^+$ were found to be particularly abundant products in the photodissociation of lithium-coated fullerenes [3–5]. The stability of $Li_7C_{60}^+$ appears to result from electronic effects: six lithium atoms donate an electron to fill the t_{1u} orbital of C_{60} to give $(Li^+)_6C_{60}^{6-}$ and the seventh lithium atom supplies the charge. On the other hand, the stability of $Li_{12}C_{60}^+$ appears to be related to a geometric effect. When fullerenes coated with the alkaline earth metals are photodissociated, $M_{32}C_{60}^+$ and $M_{37}C_{70}^+$ are particularly abundant products [4–6]. C_{60} has 20 hexagons and 12 pentagons while C_{70} has 25 hexagons and 12 pentagons. Thus the stable alkaline earth complexes appear to have one metal atom for each ring on the fullerene surface. If hundreds of alkaline earth atoms are added to C_{60}, photodissociation reveals stable structures with

* Corresponding author.

Dedicated to Professor Michael T. Bowers on the occasion of his 60th birthday.

PII S1387-3806(98)14140-4

concentric shells of 32, 104, 236, and 448 metal atoms.

Photodissociation of titanium and zirconium coated C_{60} yields particularly abundant species with 50, 62, 72, and 80 metal atoms [7]. Other transition metals show similar magic numbers. It has been suggested that these numbers are related to the number of metal atoms required to form a single layer on the fullerene using different packing schemes. Vanadium and titanium covered fullerenes evaporate metal atoms at low laser fluences, but as the fluence increases carbon loss is also observed. At high laser fluences $M_8C_{12}^+$ is the major product. $M_8C_{12}^+$ has previously been observed as a stable cluster from the reactions of early transition metals with small hydrocarbons in a cluster source [8]. Niobium and tantalum fullerene complexes were found to dissociate in a different way [9]. MC_{60}^+ (M = Ta or Nb) loses the metal atom and then the resulting C_{60}^+ dissociates by typical fullerene C_2 loss. $M_2C_{60}^+$ retains the metal atoms and dissociates by C_2 loss. While for complexes of three or more tantalum or niobium atoms, the metal atoms are retained but dissociation occurs by C_3 loss. C_3 loss is thermodynamically favored over C_2 loss if the cohesive energies of the C_{n-3}^+ and C_{n-2}^+ products are not significantly different. Fullerenes lose C_2 units [10,11] because this allows them to retain a closed cage structure while nonfullerene isomers dissociate predominantly by C_3 loss [12,13]. Based on the loss of C_3 from $M_xC_{60}^+$ ($x \geq 3$, M = Nb or Ta), it was suggested that three or more niobium or tantalum atoms destroy the fullerene cage to produce graphite sheet or ring isomers [9].

Previous studies of the structures of NbC_n^+ clusters by our group have provided compelling evidence that a niobium atom can become part of the fullerene network structure [14,15]. Thus NbC_n^+ fullerenes with odd n are much more stable than pure carbon fullerenes with odd n because the metal atom occupies the defect site in the carbon cage. Thus, loss of C_3 from $M_xC_{60}^+$ ($x \geq 3$, M = Nb or Ta) may be preferred over loss of C_2 because the metal atoms can stabilize fullerenes with an odd number of carbon atoms. In order to examine the structures of the $M_xC_{60}^+$ clusters and the $M_xC_{60-3m}^+$ fragments we have performed ion mobility measurements [16]. The mobility of an ion in an inert buffer gas depends on the average collision cross section and comparison of the measured mobilities with mobilities calculated for assumed geometries provides structural information. The application of ion mobility measurements to carbon clusters was pioneered by Bowers and collaborators. They demonstrated fullerene isomers could easily be resolved from graphite sheet and ring isomers [17]. The results presented here suggest that the fullerene cage is maintained in the presence of three or more niobium atoms. In addition, we present evidence for structural transitions in some of the $Nb_xC_{60}^+$ fullerene complexes. The most plausible interpretation of these transitions is that they result from one of the exohedral metal atoms burrowing through the fullerene cage and moving to an endohedral position.

2. Experimental methods

Except for some modifications to the source, the injected ion drift tube apparatus used for these studies has been described in detail previously [18,19] and will only be briefly discussed here. The source was modified to introduce fullerenes into the buffer gas flow, upstream from the laser vaporization region. Graphite soot was prepared by standard arc generation techniques, extracted with carbon disulfide, washed with methanol, and vacuum dried. The resulting solid was primarily C_{60}, with less than 10% C_{70} and higher fullerenes. The fullerene mixture or commercial C_{60} (99.5%, BuckyUSA) was transferred in CS_2 to a tungsten filament and the solvent was evaporated. The fullerene coated filament was mounted in the source block approximately 2 cm upstream from the niobium target (Aldrich, 99.9%). The fullerene mixture was thermally desorbed into the helium buffer gas and then mixed with the material produced by pulsed laser vaporization (308 nm) of the niobium target. Approximately 1 cm from where the clusters exit the source, a high energy electron beam is fired into the buffer gas to promote the ionization of the niobium-fullerene complexes. Ions that exit the source are focused into a quadrupole mass spectrometer where a particular

$Nb_xC_{60}^+$ ion can be selected. The mass-selected ions are focused into a low energy ion beam and injected through a small aperture into a drift tube containing neon buffer gas. As the ions enter the drift tube they undergo collisions with the buffer gas. These collisions heat the clusters, and then after their kinetic energy is thermalized, further collisions cool the clusters to the temperature of the buffer gas. At high injection energies, the clusters become hot enough that they may undergo structural transitions or even dissociate [20,21]. These processes occur close to the entrance of the drift tube so that ion mobility measurements can be used to probe the structures of the products. Neon was used as the buffer gas in these studies (instead of helium) because neon transfers more energy into internal energy as the ions are injected into the drift tube. With helium many of the ions did not fragment at the highest injection energy accessible (around 400 eV). A 2.5 cm long drift tube with 0.1 cm diameter apertures was used to study the fragmentation processes, and a 7.51 cm long drift tube with 0.025 cm apertures was used for mobility measurements. After exiting the drift tube, the ions are mass analyzed by a second quadrupole mass spectrometer and then detected by an off-axis collision dynode and dual microchannel plates.

3. Results

The mass spectrum of the ions exiting the source is dominated by C_{60}^+, but useable intensities of the $Nb_xC_{60}^+$ complexes with x up to around 5 or 6 are produced. Injection of the $Nb_xC_{60}^+$ complexes into the drift tube at elevated kinetic energies leads to dissociation. Table 1 is a summery of the main products (relative abundance ≥ 0.1) observed in the collision induced dissociation of the $Nb_xC_{60}^+$ complexes. Product branching ratios are also shown for injection energies where most of the parent ions have dissociated. Three types of dissociation process are observed: metal loss from the complex; formation of small niobium/carbon cluster ions ($Nb_xC_{2n}^+$); and the loss of small carbon fragments (C_2 or C_3). Niobium atom or niobium cluster loss is the most important

Table 1
Products from the collision induced dissociation of $Nb_xC_{60}^+$ (x = 0–5) complexes. Only the main products (relative abundance $\geq$ 0.1) are shown. Product branching ratios are shown for injection energies where most of the parent ions are dissociated

Parent cluster	Dissociation products	Branching ratio
C_{60}^+	$C_{60-2n}^+ + nC_2$	1.0
NbC_{60}^+	$Nb^+ + C_{60}$	0.6
	$C_{60}^+ + Nb$	0.4
$Nb_2C_{60}^+$	$Nb_2^+ + C_{60}$	0.5
	$Nb_nC_n^+ + Nb_{2-n}C_{60-n}$	0.3
	$Nb_2C_{60-2n}^+ + nC_2$	0.2
$Nb_3C_{60}^+$	$Nb_3^+ + C_{60}$	0.5
	$Nb_3C_{60-3n}^+ + nC_3$	0.3
	$Nb_2C_{60-2n}^+ + NbC_{2n}$	0.1
$Nb_4C_{60}^+$	$Nb_nC_n^+ + Nb_{4-n}C_{60-n}$	0.9
	$Nb_4C_{60-3n}^+ + nC_3$	0.1
$Nb_5C_{60}^+$	$Nb_5C_{60-3n}^+ + nC_3$	0.8
	$Nb_nC_n^+ + Nb_{5-n}C_{60-n}$	0.2

dissociation pathway for clusters with $x \leq 3$. Small $Nb_xC_n^+$ fragments are first observed for $Nb_2C_{60}^+$, and become the dominant dissociation product for $Nb_4C_{60}^+$. Loss of C_3 is observed for all $Nb_xC_{60}^+$ complexes with $x = 3$–5 but it is the dominant dissociation process for only $Nb_5C_{60}^+$. Loss of C_2 is a minor dissociation pathway for $Nb_2C_{60}^+$.

Fig. 1 shows a plot of the injection energy dependence of the fragmentation processes. The injection energy threshold for dissociation of C_{60}^+ is at 260–300 eV. The threshold for NbC_{60}^+ is much lower, at 120–160 eV. The threshold for dissociation of $Nb_2C_{60}^+$ is broad, with a tail extending up to 300 eV, while the thresholds for $Nb_3C_{60}^+$ and $Nb_4C_{60}^+$ are narrow and occur at 260–300 eV, close to the threshold for C_{60}^+. The threshold for $Nb_5C_{60}^+$ is at a slightly higher injection energy that for C_{60}^+. These results indicate that for NbC_{60}^+ and for most of the $Nb_2C_{60}^+$ complexes, the dissociation energy is considerably smaller than for C_{60}^+. While for $Nb_3C_{60}^+$, $Nb_4C_{60}^+$, and $Nb_5C_{60}^+$ the dissociation energies are similar to that of C_{60}^+.

Ion mobility measurements were performed by injecting 50 μs pulses of mass selected ions into the drift tube and recording the arrival time distribution at

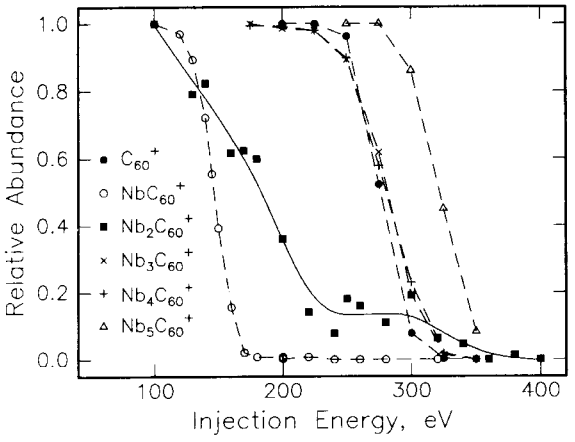

Fig. 1. Plot of the injection energy dependence of the dissociation of C_{60}^+ and $Nb_xC_{60}^+$ complexes with $x = 1$–5. The results were obtained with the short drift tube and a neon buffer gas pressure of around 0.6 Torr. The points are the experimental data, the lines are guides.

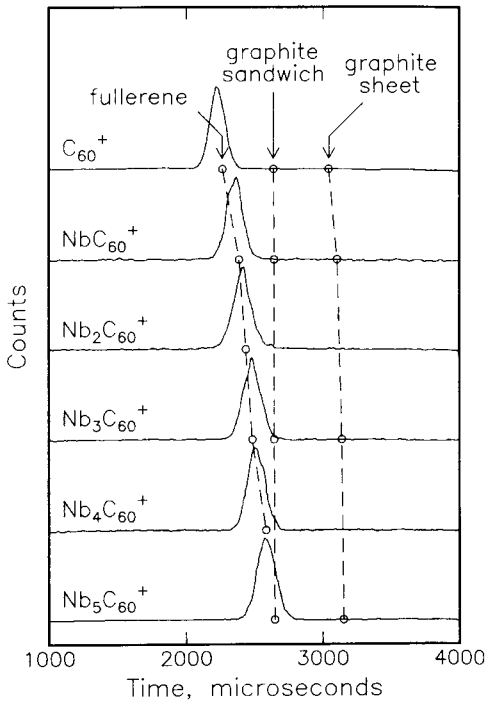

Fig. 2. Low injection energy drift time distributions for C_{60}^+ and $Nb_xC_{60}^+$ complexes with $x = 1$–5. The distributions were recorded with the long drift tube and a neon buffer gas pressure of around 5.0 Torr. Calculated drift times for $Nb_xC_{60}^+$ fullerenes, graphite sandwiches, and graphite sheets are shown by the points (see text).

the detector with a multichannel scaler. A neon buffer gas pressure of ~5 Torr was employed, along with a drift field of 13.2 V/cm. The arrival time distributions are converted into drift time distributions by correcting the time scale so that it only reflects the time the ions spend traveling through the drift tube [18]. Drift time distributions measured for $Nb_xC_{60}^+$ at low injection energies are plotted in Fig. 2. As the number of niobium atoms increase, the drift times steadily increase.

Reduced mobilities were determined from the drift time distributions using [22]

$$K_o = \frac{L^2}{t_D V} \frac{p}{760} \frac{273.15}{T} \quad (1)$$

where L is the length of the drift tube, t_D is the drift time, V is the voltage across the drift tube, p is the buffer gas pressure in Torr, and T is the temperature. Fig. 3 shows the measured inverse reduced mobilities for $Nb_xC_{60}^+$ ($x = 0$–5) plotted as a function of injection energy. The inverse reduced mobility is plotted because it is directly proportional to the collision cross section of the cluster. The inverse reduced mobility of C_{60}^+ is constant over the range of injection energies employed, indicating that C_{60}^+ maintains the structure of the spherical fullerene even after injection at energies that are high enough to dissociate most of the ions. The inverse reduced mobility of NbC_{60}^+ is significantly (5.8%) larger than for C_{60}^+, which confirms that the niobium atom is exohedral. The inverse reduced mobility of NbC_{60}^+ remains constant until this complex is completely dissociated. For $Nb_xC_{60}^+$ ($x \geq 2$) the stepwise increase in the inverse mobilities at low injection energy on going from $Nb_xC_{60}^+$ to $Nb_{x+1}C_{60}^+$ suggests that the additional niobium atoms are also added to the outside of the fullerene. As the injection energy is increased, the inverse mobilities of the $Nb_xC_{60}^+$ complexes with $x \geq 2$ decrease, indicating the complexes become more compact. Note that the inverse mobility of $Nb_2C_{60}^+$ decreases to the value for the NbC_{60}^+ complex.

Drift time distributions for $Nb_3C_{60}^+$ and the fragments resulting from sequential C_3 loss, $Nb_3C_{57}^+$ to $Nb_3C_{42}^+$, are shown in Fig. 4. Each drift time distribu-

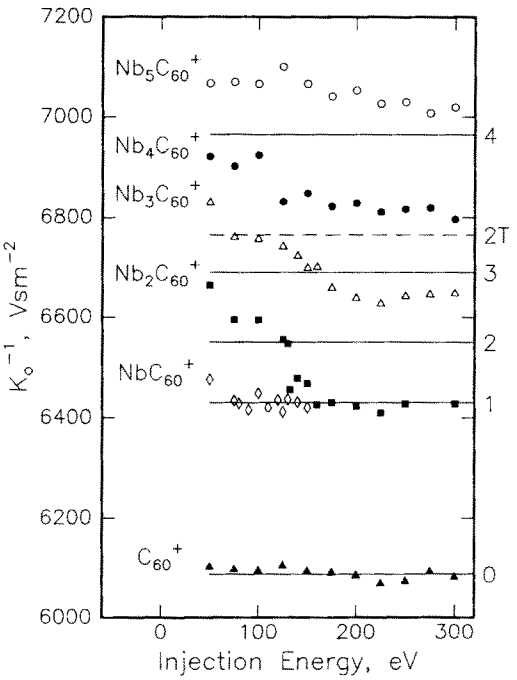

Fig. 3. Inverse mobilities for C_{60}^+ and $Nb_xC_{60}^+$ complexes with x = 1–5 plotted as a function of the injection energy. The distributions were recorded with the long drift tube and a neon buffer gas pressure of around 5.0 Torr. The points are the experimental data and the lines show inverse mobilities calculated for geometries discussed in the text. The solid lines show inverse mobilities calculated for geometries where the niobium atoms form a compact cluster on the fullerene surface. The dashed line labelled 2T shows the calculated inverse mobility for a $Nb_2C_{60}^+$ geometry where the niobium atoms are attached to opposite sides of the fullerene cage.

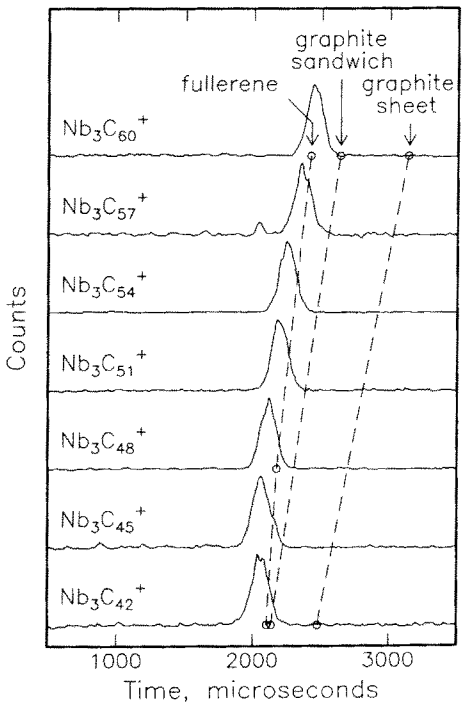

Fig. 4. Drift time distributions measured at high injection energies for $Nb_xC_{60}^+$ and the fragments $Nb_3C_{57}^+$ to $Nb_3C_{42}^+$. The distributions were recorded with the long drift tube and a neon buffer gas pressure of around 5.0 Torr. Calculated drift times for $Nb_2(Nb@C_{60-3n})^+$ fullerenes, graphite sandwiches, and graphite sheets are shown by the points (see text).

tion shows a single peak with a width close to that expected for a single isomer. The drift time distribution for $Nb_3C_{60}^+$ was recorded at high injection energy and so this distribution is for the more compact (high injection energy) isomer apparent in Fig. 3. The drift times of $Nb_3C_{57}^+$ to $Nb_3C_{42}^+$ steadily shift to shorter times.

4. Discussion

Collisional excitation of $Nb_xC_{60}^+$ clusters in neon results in fragmentation products that are similar to those observed in the photodissociation experiments of Martin and collaborators [9]. In particular, we have confirmed the unusual fragmentation process, loss of C_3, reported by this group for $Nb_xC_{60}^+$ clusters with $x \geq 3$. In order to obtain more information about the structures of the $Nb_xC_{60}^+$ clusters and their fragmentation products, we have calculated mobilities for a variety of simple structural models for comparison with the experimental data. Mobilities were calculated using the exact hard spheres scattering model [23]. If the structure is correct, the calculated mobility is expected to be within 2% of the measured value. However, agreement with the measured mobility is not proof that the structure is correct, because other low energy structures could have the same mobility. In order to calculate mobilities using the exact hard spheres scattering model, it is necessary to define hard sphere contact distances for C–Ne and Nb–Ne interactions. The hard sphere contact distance for C–Ne

interactions (3.4 Å) was determined by fitting the measured mobility for C_{60}^+. An estimate of the Nb–Ne hard sphere contact distance was obtained by modeling the NbC_{60}^+ complex. The fact that the inverse mobility of NbC_{60}^+ is significantly larger than for C_{60}^+ indicates that this complex is exohedral. The most likely Nb–C_{60} bonding geometry is an η–2 bridge over the 6–6 double bond of C_{60}. An arene complex with the metal over a hexagon of the fullerene is a plausible alternative. However, we do not know of any direct experimental evidence for metal arene complexation of C_{60} or for niobium arene complexes. Some model structures for the Nb-bridged geometry were optimized at the Hartree-Fock level using the Gaussian 92 package. The complex was modeled using ethylene, naphthalene, and C_{60} fragments with up to 30 carbon atoms. These models all gave a 2.0 Å distance between the niobium atom and the center of the double bond. To fit the Nb-bridged structure to the measured inverse mobility for the NbC_{60}^+ complex required a Nb–Ne contact distance of 3.6 Å.

Drift times calculated for several isomers using assumed geometries and the exact hard spheres scattering model [23] are shown in Fig. 2. In addition to the results shown in the figure, calculations were also performed for some ring isomers. The calculated drift times for the ring isomers are out of the range of the plot and so these isomers can be ruled out. As can be seen from the figure, planar graphite sheet structures are expected to occur at much longer drift times than the observed features. This is true regardless of the arrangement of the niobium atoms. So isomerization of the $Nb_xC_{60}^+$ clusters into graphite sheet structures can also be ruled out. Calculated drift times for "graphite sandwiches," two stacked graphite fragments with niobium atoms sandwiched between them, are shown in the figure because these structures have mobilities that are similar to those of the fullerenes. The graphite sandwiches are energetically unfavorable because of the large number of dangling bonds around their edges. The 3.35 Å bulk graphite sheet spacing was used for these structures to calculate their drift times even though inclusion of the niobium atoms between the sheets would most likely result in a larger separation. The calculated drift times for the "graphite sandwiches" are larger than for the observed features, and a greater sheet separation would increase the discrepancy. It seems that only Nb_x-fullerene models accurately predict the observed drift times. The fullerene models will now be described in detail.

Quantum chemical calculations were not attempted for $Nb_xC_{60}^+$ adducts with $x \geq 2$. Instead we constructed some plausible model structures assuming that the niobium clusters were constrained to the geometries determined by Goodwin and Salahub [24] and placed at a 2.0 Å Nb–C=C distance from the fullerene. This first order modeling does not consider changes in the geometries of the niobium cluster or the fullerene due to their complexation. Assuming $Nb_2C_{60}^+$ has both niobium atoms exohedral (which is qualitatively consistent with the increase in inverse mobility on going from NbC_{60}^+ to $Nb_2C_{60}^+$ at low injection energy) two structures can be imagined: a C_{60} with trans-Nb atoms and a C_{60} with an Nb_2 dimer. Placing two 6–6 bond bridging niobium atoms on opposite sides of the fullerene cage would maximize the inverse mobility of the complex. This bonding scheme has been reported for some palladium [25–27] and platinum [25,26] complexes. The predicted inverse mobility for this structure (line 2T in Fig. 3) is significantly larger than the value measured for $Nb_2C_{60}^+$ at low injection energy. Placing a niobium dimer on the surface of the fullerene provides the most compact geometry for two exohedral niobium atoms. Based on known ruthenium [28] and iridium [29] dimer-fullerene complexes, the niobium dimer (with a 2.10 Å bond length) was placed over two 6–6 bonds of a single fullerene hexagon. This structure has a calculated inverse mobility (line 2 in Fig. 3) within 0.5% of the inverse mobilities measured at low injection energies.

Similar modeling of the $Nb_3C_{60}^+$, $Nb_4C_{60}^+$, and $Nb_5C_{60}^+$ complexes also indicate that the niobium atoms cluster on the surface of the fullerene. For $Nb_3C_{60}^+$ the Nb_3 was added η–2,η–2,η–2 over the 6–6 bonds on a single fullerene hexagon. This geometry is patterned after the structure of a known Ru_3–C_{60} complex [30]. This simple model agreed with the experimental data within 1% (line 3 in Fig. 3). Placing three niobium atoms randomly on the

fullerene surface results in an inverse mobility over 5% larger than observed. For $Nb_4C_{60}^+$, a geometry with a terahedral Nb_4 bound by its three base atoms η–2,η–2,η–2 on a single hexagon of the fullerene, has a calculated inverse mobility within 1% of the experimental value (line 4 in Fig. 3). Once again, a random distribution of niobium atoms greatly over estimates the inverse mobility (by around 8%). For the $Nb_5C_{60}^+$ complex the calculated inverse mobility for a geometry with a niobium dimer and trimer on the fullerene surface is within 1% of the experimental value, while the calculated inverse mobility for a geometry with randomly distributed niobium atoms is 10% too large. These results clearly show that the niobium atoms must be clustered together and not randomly dispersed on the fullerene surface. However, we are not able to determine the precise structure of the $Nb_xC_{60}^+$ complexes because small changes in the bond lengths within the niobium cluster and between the cluster and fullerene can change the cross sections by 1%–2%.

The inverse mobilities for the $Nb_2C_{60}^+$ complex decrease as the injection energy is raised and for injection energies greater than around 140 eV, the inverse mobility approaches the value for NbC_{60}^+. This indicates that a structural transition is occurring and the $Nb_2C_{60}^+$ complex is rearranging to a more compact geometry. This structural transition could be the exohedral niobium atoms rearranging into more compact configuration on the fullerene surface, one or both of the niobium atom being incorporated into the cage network, or an exohedral niobium atom being incorporated inside the cage. Rearrangement of the niobium atoms on the fullerene surface seems unlikely because the modeling described above indicates that the niobium atoms are already in a compact dimer geometry. To examine the possibility of networked niobium structures (structures where a niobium atom is part of the cage) we replaced two carbon atoms in a C_{62} cage by a niobium atom. The calculated inverse mobilities for this structure was around 5% larger than the measured values at high injection energies. The relatively large inverse mobility for this structure results because the niobium atom still protrudes from the fullerene surface because of the relatively long Nb–C bonds. So the only remaining explanation is that the niobium dimer is capable of activating the fullerene, and one of the niobium atoms penetrates into the fullerene to form a $Nb(Nb@C_{60})^+$ complex. The endohedral niobium would not contribute to the cross section since it is hidden from the buffer gas by the surrounding C_{60}. Such a complex would be expected to have approximately the same inverse mobility as NbC_{60}^+, in agreement with the experiment results. Therefore, it appears that niobium clusters can activate the fullerene cage and form a complex with an endohedral niobium atom. For $Nb_2C_{60}^+$, the proposed activation of the fullerene cage to form an endohedral complex apparently competes with dissociation and this is probably responsible for the broad dissociation threshold observed for this complex (see Fig. 1). The endohedral $Nb(Nb@C_{60})^+$ complex is presumably more strongly bound than the exohedral complex and once it is formed it can survive to higher injection energies.

The inverse mobilities for $Nb_xC_{60}^+$ (x = 3–5) also decrease at high injection energies suggesting that they also undergo a transition to an endohedral $Nb_{x-1}(Nb@C_{60})^+$ geometry. However, for these complexes the inverse mobilities do not return completely to the values of the $Nb_{x-1}C_{60}^+$ complexes at low injection energies. So the interpretation of the structural transitions observed for $Nb_xC_{60}^+$ with $x \geq 3$ is not as straight forward as for $Nb_2C_{60}^+$. It is possible that the arrangement of the niobium atoms on the fullerene surface is different in the $Nb_x(Nb@C_{60})^+$ and $Nb_xC_{60}^+$ complexes with $x \geq 2$. Note that a transition to an endohedral geometry is not observed for NbC_{60}^+. A single metal atom may not be able to catalyze this structural transformation. On the other hand, the structural transition competes with dissociation for $Nb_2C_{60}^+$, and occurs at energies below the dissociation threshold for $Nb_xC_{60}^+$, $x \geq 2$. So an alternative explanation for the absence of the proposed endohedral transition for NbC_{60}^+ is that a single metal atom is not bound to the fullerene strongly enough for the NbC_{60}^+ to survive to sufficiently high energies for the transition to occur. In the $Nb_xC_{60}^+$ complexes the Nb_x clusters are bound to the fullerene surface with more chemical bonds, and so these

complexes survive to higher energies. The mechanism by which the niobium atom moves to an endohedral position seems to be different from other processes that lead to the formation of endohedral fullerenes. For example, it is known that rare gas atoms [31] and alkali metal atoms [32,33] can be forced into a fullerene cage by kinetic energy. Rare gas atoms have also been driven into C_{60} by high pressure and temperature [34]. In work that seems more closely related to that described here, McElvany has reported formation of $Y@C_{60}^+$ from laser vaporization of graphite/C_{60}/Y_2O_3 mixtures [35]. However, the mechanism and the intermediates involved in this process remain unknown.

The results described above indicate that the simple addition of three or more niobium atoms to C_{60} does not result in destruction of the fullerene cage. But the possibility still exists that the complexes may isomerize upon dissociation. Drift time distributions for $Nb_3C_{60}^+$ and the fragments $Nb_3C_{57}^+$ and $Nb_3C_{42}^+$ are shown in Fig. 4. In the top distribution, $Nb_3C_{60}^+$ is the compact (high injection energy) structure discussed above. This isomer probably has an $Nb_2(Nb@C_{60})^+$ structure. The drift times of the fragments, $Nb_3C_{57}^+$ to $Nb_3C_{42}^+$, become slightly smaller each time the complex loses three carbon atoms in a dissociation step. Predicted drift times for the graphite sheet, "graphite sandwich," and $Nb_2(Nb@C_{60-3n})^+$ fullerene structures are shown in the figure. The predicted drift times of ring structures (not shown) are at much longer times. The "graphite sandwiches" are once again restricted to the bulk graphite spacing which minimizes their cross sections. However, they are still at slightly larger drift times than the measured features. The $Nb_2(Nb@C_{60-3n})^+$ fullerene geometry fits the measured drift times of the parent and fragments. An $Nb_{x-1}(Nb@C_{60-3n})^+$ fullerene geometry also provides the best fit to the mobilities of the products of $Nb_4C_{60}^+$ and $Nb_5C_{60}^+$ fragmentation.

For carbon rings and other nonfullerene geometries, the preferred dissociation process is loss of C_3 rather than C_2 because of the high stability of C_3 fragment [36]. C_2 loss dominates in fullerene dissociation because the energetic disadvantage of losing C_2 over C_3 is compensated by maintaining a stable fullerene structure with an even number of carbon atoms [11]. Fullerenes with an odd number of carbon atoms are unstable because they have a defect, a missing atom, in the cage. As noted above, a plausible explanation for the unusual C_3 loss process observed for the $Nb_xC_{60}^+$, $x \geq 3$, complexes is suggested by previous ion mobility studies of niobium doped carbon clusters performed in this laboratory [13,14]. In those experiments fullerenes with an NbC_{2n-1}^+ composition were identified. Based on their mobility and reactivity, the geometry assigned to these species was a C_{2n} fullerene structure with one of the carbons replaced by a niobium atom. The ability of the niobium atom to substitute into the fullerene cage structure, may allow $Nb_xC_{60}^+$, $x \geq 3$, complexes to fragment by loss of C_3 and still maintain the stable fullerenelike structure. The next C_3 loss step would allow the cage to return to a pure carbon fullerene structure. This process can then repeat until the cluster is too small to retain the fullerene geometry. In Fig. 4, the mobilities of the fragments smoothly shift to slightly shorter time with each dissociation step. This behavior is expected even if the fragments with an odd number of carbon atoms have a niobium atom occupying the defect site in the fullerene cage. The mobilities of a networked NbC_n^+ fullerene with an odd number of carbon atoms is expected to be very similar to the mobilities of exohedral NbC_{n-1}^+ and NbC_{n+1}^+ fullerenes, because the niobium atom still protrudes from the fullerene surface. It is worth noting that C_3 loss is not observed for $x < 3$, indicating that three or more niobium atoms are required for this process. This is probably just a reflection of the fact that a cluster of several niobium atoms is required for their binding energy to the fullerene to be large enough for the complex to survive at the high internal energies required for dissociation.

5. Conclusions

Ion mobility measurements indicate that the niobium atoms in $Nb_xC_{60}^+$ complexes cluster together on the surface of the fullerene. Upon collisional heating,

the inverse mobility of $Nb_xC_{60}^+$ ($x \geq 2$) complexes decrease to approach the inverse mobility of the unannealed complex with one less niobium atom. The most likely explanation for this structural transition is that the niobium clusters activate the fullerene cage and allow a niobium atom to pass through and form an endohedral niobium, $Nb_{x-1}(Nb@C_{60})^+$, complex. Formation of such an endohedral complex is not observed for NbC_{60}^+, indicating that more than one niobium atom is required to facilitate formation of the endohedral complex. $Nb_3C_{60}^+$ retains a fullerenelike geometry when it dissociates even though the complex displays an anomalous C_3 fragmentation pattern. It is likely that a niobium atom occupies the defect site in the fullerene cage allowing the parent to dissociate by the thermodynamically preferred C_3 loss process while maintaining a stable fullerenelike geometry.

Acknowledgement

We gratefully acknowledge the support of this work by the National Science Foundation.

References

[1] L.M. Roth, Y. Huang, J.T. Schwedler, C.J. Cassady, D. Ben-Amotz, B. Kahr, B.S. Freiser, J. Am. Chem. Soc. 113 (1991) 6298; Y. Huang, B.S. Freiser, J. Am. Chem. Soc. 113 (1991) 8186; Y. Huang, B.S. Freiser, J. Am. Chem. Soc. 113 (1991) 9418.
[2] J.E. Reddic, J.C. Robinson, M.A. Duncan, Chem. Phys. Lett. 279 (1997) 203.
[3] T.P. Martin, N. Malinowski, U. Zimmermann, U. Näher, H. Schaber, J. Phys. Chem. 99 (1993) 4210.
[4] U. Zimmermann, N. Malinowski, A. Burkhardt, T.P. Martin, Carbon 33 (1995) 995.
[5] T.P. Martin, U. Zimmermann, N. Malinowski, M. Heinebrodt, S. Frank, F. Tast, Phys. Scr. T66 (1996) 38.
[6] U. Zimmermann, N. Malinowski, U. Näher, S. Frank, T.P. Martin, Phys. Rev. Lett. 72 (1994) 3542.
[7] F. Tast, N. Malinowski, S. Frank, M. Heinebrodt, I.M.L. Billas, T.P. Martin, Z. Phys. D 40 (1997) 351.
[8] B.C. Guo, S. Wei, J. Purnell, S. Buzza, A.W. Castleman, Science 256 (1992) 515.
[9] F. Tast, N. Malinowski, S. Frank, M. Heinebrodt, I.M.L. Billas, T.P. Martin, Phys. Rev. Lett. 77 (1996) 3529.
[10] L.A. Bloomfield, M.E. Geusic, R.R. Freeman, W.L. Brown, Chem. Phys. Lett. 121 (1985) 33.
[11] S.C. O'Brien, J.R. Heath, R.F. Curl, R.E. Smalley, J. Chem. Phys. 88 (1988) 220.
[12] M.E. Geusic, T.J. McIlrath, M.F. Jarrold, L.A. Bloomfield, R.R. Freeman, W.L. Brown, J. Chem. Phys. 84 (1986) 2421.
[13] P.P. Radi, T.L. Bunn, P.R. Kemper, M.E. Molchan, M.T. Bowers, J. Chem. Phys. 88 (1988) 2809.
[14] D.E. Clemmer, J.M. Hunter, K.B. Shelimov, M.F. Jarrold, Nature 372 (1994) 248.
[15] D.E. Clemmer, M.F. Jarrold, J. Am. Chem. Soc. 117 (1995) 8841.
[16] D.F. Hagen, Anal. Chem. 51 (1979) 870; G. von Helden, M.-T. Hsu, P.R. Kemper, M.T. Bowers, J. Chem. Phys. 95 (1991) 3835; R.H. St. Louis, H.H. Hill, Crit. Rev. Anal. Chem. 21 (1990) 321; D.E. Clemmer, M.F. Jarrold, J. Mass Spectrom. 32 (1997) 577.
[17] G. von Helden, M.-T. Hsu, N. Gotts, M.T. Bowers, J. Phys. Chem. 97 (1993) 8182.
[18] M.F. Jarrold, J.E. Bower, K. Creegan, J. Chem. Phys. 90 (1989) 3615.
[19] M.F. Jarrold, J.E. Bower, J. Chem. Phys. 96 (1992) 9180.
[20] M.F. Jarrold, E.C. Honea, J. Phys. Chem. 95 (1991) 9181.
[21] M.F. Jarrold, E.C. Honea, J. Am. Chem. Soc. 114 (1992) 459.
[22] E.A. Mason, E.W. McDaniel, Transport Properties of Ions in Gases, Wiley, New York, 1988.
[23] A.A. Shvartsburg, M.F. Jarrold, Chem. Phys. Lett. 261 (1996) 86.
[24] L. Goodwin, D. Salahub, Phys. Rev. A 47 (1993) R774.
[25] P.J. Fagan, J.C. Calabrese, B. Malone, J. Am. Chem. Soc. 113 (1991) 9408.
[26] P.J. Fagan, J.C. Calabrese, B. Malone, Acc. Chem. Res. 25 (1992) 134.
[27] C. Bo, M. Costas, J.M. Poblet, J. Phys. Chem. 99 (1995) 5914.
[28] M. Rasinkangas, T.T. Pakkanen, T.A. Pakkanen, M. Algrén, J. Rouvinen, J. Am. Chem. Soc. 115 (1993) 4901.
[29] I.P. Mavunkal, Y. Chi, S.-M. Peng, G.-H. Lee, Organometallics 14 (1995) 4454.
[30] H.-F. Hsu, J.R. Shapley, J. Am. Chem. Soc. 118 (1996) 9192.
[31] T. Weiske, D.K. Böhme, J. Hrušák, W. Krätschmer, H. Schwarz, Angew. Chem. Int. Ed. Engl. 30 (1991) 884.
[32] Z. Wan, J.F. Christian, S.L. Anderson, Phys. Rev. Lett. 69 (1992) 1352.
[33] R. Tellgmann, N. Krawez, S.-H. Lin, I.V. Hertel, E.E.B. Campbell, Nature 382 (1996) 407.
[34] M. Saunders, H.A. Jiménez-Vázquez, R.J. Cross, R.J. Poreda, Science 259 (1993) 1428.
[35] S.W. McElvany, J. Phys. Chem. 96 (1992) 4935.
[36] K. Raghavachari, J.S. Binkley, J. Chem. Phys. 87 (1987) 2191.